

Adaptive Instantiation of the Protocol Interference Model in Wireless Networked Sensing and Control

Xin Che, *Student Member, IEEE*, Hongwei Zhang, *Member, IEEE*, Xi Ju, Xiaohui Liu

Abstract—Interference model is the basis of MAC protocol design in wireless networked sensing and control, and it directly affects the efficiency and predictability of wireless messaging. To exploit the strengths of both the physical and the protocol interference models, we analyze how network traffic, link length, and wireless signal attenuation affect the optimal instantiation of the protocol model. We also identify the inherent tradeoff between reliability and throughput in the model instantiation. Our analysis sheds light on the open problem of efficiently optimizing the protocol model instantiation. Based on the analytical results, we propose the physical-ratio-K (PRK) interference model as a reliability-oriented instantiation of the protocol model. Via analysis, simulation, and testbed-based measurement, we show that PRK-based scheduling achieves a network throughput very close to (e.g., 95%) what is enabled by physical-model-based scheduling while ensuring the required packet delivery reliability. The PRK model inherits both the high fidelity of the physical model and the locality of the protocol model, thus it is expected to be suitable for distributed protocol design. These findings shed new light on wireless interference models; they also suggest new approaches to MAC protocol design in the presence of uncertainties in traffic patterns and application QoS requirements.

Index Terms—Wireless interference model, protocol model, physical model, throughput, reliability, local adaptation, analysis, measurement, simulation, control theory

I. INTRODUCTION

With the development of networked embedded sensing and control, wireless networks are increasingly applied to mission-critical applications such as industrial monitoring and control [1]. This is evidenced by the recent industry standards such as WirelessHART [2] and ISA SP100.11a [3] which target wireless networked sensing and instrumentation. In supporting real-time, mission-critical tasks, these wireless networks are required to ensure real-time, reliable data delivery. Nonetheless, wireless communication is subject to various dynamics and uncertainties. Due to the broadcast nature of wireless communication, in particular, concurrent transmissions may interfere with one another and introduce co-channel interference. Co-channel interference not only reduces the reliability and throughput of wireless networks, it also increases the variability and uncertainty in data communication [4], [5], [6]. Therefore, effectively scheduling concurrent transmissions to control co-channel interference has become critical for enabling reliable, predictable wireless communication.

This work is supported in part by NSF awards CNS-1054634, CNS-1136007, and GENI-1633, as well as grants from Ford Research and GM Research. An extended abstract containing some preliminary results of this paper appeared in IEEE SECON 2010.

Xin Che, Hongwei Zhang, Xi Ju, and Xiaohui Liu are with the Department of Computer Science, Wayne State University, U.S.A. E-mail: {chexin, hongwei, xiju, xiaohui}@wayne.edu.

A basis of interference control is the interference model which *predicts* whether a set of concurrent transmissions may interfere with one another. Two commonly used models are the physical interference model and the protocol interference model [7]. In the physical model, a set of concurrent transmissions are regarded as not interfering with one another if the resulting signal-to-interference-plus-noise-ratio (SINR) at every receiver is no less than a threshold value γ_0 ; in the protocol model, a transmission is regarded as not being interfered by an interferer if the interferer is at least K times the transmitter-receiver distance away from the receiver¹. For simplicity, we also call the physical model the *SINR model* and the protocol model the *ratio-K model* in this paper, and we regard scheduling based on the SINR model and the ratio-K model SINR-based scheduling and ratio-K-based scheduling respectively.

The SINR model is based on communication theory, and it can be regarded as an instantiation of the graded-SINR model [9] for satisfying certain minimum link reliability. The SINR model is a high fidelity model in general, but the interference relations defined by it are non-local and combinatorial. This is because whether one transmission interferes with another is modeled as *explicitly* depending on all the other transmissions in the network. Accordingly, SINR-based scheduling usually requires network-wide coordination. Since the coordination delay slows down protocol convergence [10], [11] and increases uncertainty [12], it is difficult to use the SINR model in *distributed* protocol design. This is especially the case when network traffic pattern and environmental conditions are dynamic and potentially unpredictable.

Unlike the SINR model, the ratio-K model defines local, pair-wise/non-combinatorial interference relations where interference is regarded as existent only between nodes in a local neighborhood. Accordingly, the ratio-K model is suitable for distributed protocol design since ratio-K-based scheduling only requires coordination among nodes in their local neighborhood. The locality of ratio-K-based scheduling can also enable agile protocol adaptation for addressing the challenges of unpredictable traffic pattern and environmental dynamics. Nonetheless, the ratio-K model is an approximate model in nature, and it does not ensure reliable data delivery in general. For instance, the RTS-CTS-based channel access control can only enable a data delivery ratio of $\sim 50\%$ in our field wireless sensor networks [13], [14]; via testbed-based measurement study of event-detection sensor networks, Choi et al. have also shown that CSMA- and RTS-CTS-based channel access control mechanisms may only enable a data delivery ratio of 16.9% and

¹We replace the original notation of $(1 + \Delta)$ [7] with K for simplicity. Also note that the commonly used K-hop model [8] is a special case of the protocol model in geometric graphs.

36.8% respectively [15].

To enable the design of distributed MAC protocols for agile, predictable interference control, an *open question* is whether it is possible to develop an interference model that has both the locality of the ratio-K model and the high fidelity of the SINR model. Given that the ratio-K model is local and can enable agile, distributed protocols, we explore the possibility of extending the ratio-K model to preserve its locality while addressing the low performance issue of ratio-K-based scheduling. To this end, we first study the behavior of ratio-K-based scheduling, and a summary of our findings are as follows:

- We analyze how network traffic load, link length, and wireless signal attenuation affect the effective instantiation of the ratio-K model. We find that fixing K to a constant number, as in most existing studies [16], [9], [17], can lead to significant performance loss when network and environmental settings change. For instance, deviation from the optimal K by up to 1 can cause up to 68% throughput loss, and fixing K to 2 may lead to a link reliability less than 80%. These findings suggest that it is important to choose the right K when studying ratio-K-based scheduling, otherwise the performance evaluation will be biased.
- We also find that there is inherent tradeoff between reliability and throughput when instantiating the ratio-K model. Maximum network throughput is usually achieved not at the minimum K for ensuring certain link reliability, but at a smaller K. For instance, $\sqrt{2}$ is the optimal K for maximizing throughput in many scenarios, but, with non-negligible probability, $\sqrt{2}$ is unable to guarantee an 80% link reliability. Moreover, as K increases from the minimum one required for satisfying certain link reliability, network throughput tends to decrease, especially when link reliability requirement is high.

Our findings (in particular, those on the reliability-throughput tradeoff in ratio-K-based scheduling) suggest that, in wireless networked sensing and control where high link reliability is critical not only for reliable data delivery but also for small latency and latency jitter, we can use link reliability requirement as the basis of instantiating the ratio-K model. Accordingly, we propose the *physical-ratio-K (PRK) interference model* as a reliability-oriented instantiation of the ratio-K model, where the link-specific choice of K adapts to network and environmental conditions as well as application QoS requirements to ensure certain minimum reliability of every link.

To understand the potential effectiveness of PRK-based medium access control, we analyze the performance of PRK-based scheduling. We find that, for a given requirement on link reliability, PRK-based scheduling achieves a network spatial throughput very close to what is enabled by SINR-based scheduling, for instance, at least 95% in many scenarios we study. Moreover, as link reliability requirement increases, the throughput loss in PRK-based scheduling further decreases. Since link reliability is a locally measurable metric, reliability-oriented selection of K in PRK-based medium access control enables link-specific, local search of K via feedback on packet delivery reliability. This suggests new approaches to MAC protocol design in the presence of unpredictable traffic patterns,

for instance, by letting the receiver of each link locally choose a K for satisfying application-specific link reliability requirement. This also addresses the challenge of how to efficiently adapt K according to dynamic, potentially unpredictable network and environmental settings, which has been recognized as an open problem by Shi *et al.* [18] who studied the ratio-K model in parallel with our work here.

The above analytical results give us insight into the behavior of ratio-K-based scheduling in uniform grid and random networks with a wide range of system configurations (on factors such as traffic load, link length, and wireless signal attenuation). We have verified these results through simulation as well as measurement study in both the NetEye and the MoteLab wireless sensor network testbeds which reflect real-world properties such as non-uniform network settings.

The rest of the paper is organized as follows. In Section II, we present the wireless channel and radio models used in the analytical part of this paper. We study how system properties and optimization objectives affect the ratio-K model instantiation in Section III, and we examine the optimality of PRK-based scheduling in Section IV. We corroborate our analytical results through testbed-based measurement in Sections V; we have also validated the analytical results through comprehensive simulation, and interested readers can find the detailed simulation results in [19]. We discuss related work in Section VI and make concluding remarks in Section VII.

II. PRELIMINARIES

In this section, we present the wireless channel and radio models used in the analytical part of this paper.

Channel model. To characterize signal attenuation in wireless networks, we use the log-normal path loss model [20] which is widely adopted in protocol design and analysis. By this model, the power P_r of the received signal at a node distance d away from the transmitter is computed as follows:

$$P_r = P_t - PL(d_0) - 10\alpha \log_{10} \frac{d}{d_0} + N(0, \sigma^2) \quad (1)$$

where P_t is the transmission power, $PL(d_0)$ is the power decay at the reference distance d_0 , α is the path loss exponent, $N(0, \sigma)$ is a Gaussian random variable with mean 0 and variance σ . In our study, we use different instantiations of α and σ to represent different wireless environments.

Radio model. The reception capability of a radio can be characterized by the bit error rate (BER) and the packet delivery rate (PDR) in decoding signals with specific signal-to-interference-plus-noise-ratios (SINR). Focusing on wireless sensing and control networks, we base our study mainly on the commonly-used, IEEE 802.15.4-compatible CC2420 radios; we also study low-power UWB radios which are expected to be used for intra-vehicular sensing and control [21], and we observe similar results. Due to the limitation of space, we relegate the results on UWB radios to [19]. For CC2420 radio, the BER for a SINR of γ is computed as follows [22]:

$$\text{BER}(\gamma) = \frac{8}{15} \times \frac{1}{16} \times \sum_{k=2}^{16} (-1)^k \binom{k}{16} e^{(20 \times \gamma \times (\frac{1}{k} - 1))} \quad (2)$$

Accordingly, the PDR for a SINR of γ is computed as follows:

$$\text{PDR}(\gamma, f) = (1 - \text{BER}(\gamma))^{8f} \quad (3)$$

where f is the packet length (in units of bytes) including overhead such as packet header.

Remark. For analytical tractability, the aforementioned models do not capture all the real-world phenomena such as the irregularity in wireless communication [23]. But the analysis based on these models gives us insight into wireless interference models, and the analytical results have also been verified through testbed-based measurement which captures complex real-world phenomena as we discuss in Section V.

III. INSTANTIATION OF THE RATIO-K MODEL

To explore effective methods of instantiating the ratio-K model, we first analyze the performance of ratio-K-based scheduling, then we numerically study how system properties and optimization objectives affect the effective instantiation of the ratio-K model.

A. Performance of ratio-K-based scheduling

Here we analyze network throughput and link reliability in ratio-K-based scheduling when the ratio-K model is instantiated with different Ks. Focusing on link-layer behavior, we consider the optimization objective of maximizing channel spatial reuse (i.e., maximizing the number of concurrent transmissions) in ratio-K-based scheduling. In Sections III and IV accordingly, by network throughput, we mean network spatial throughput as defined by Formula (4); in our measurement study in Section V, we consider end-to-end throughput which directly reflects network-wide behavior.

Towards characterizing the computational complexity of ratio-K-based scheduling in general, we first prove that the ratio-K-based scheduling is NP-complete as follows:

Proposition 1: The problem of maximizing the number of interference-free concurrent transmissions is NP-complete when the interference model is the ratio-K model. \square (Interested readers can find the proof in [19].)

We consider both grid and Poisson random networks in our analysis, but, given the NP-completeness of general ratio-K-based scheduling, we only consider the following special cases of the problem for computational tractability and for deriving closed-form formula for the optimal scheduling performance:

- To avoid the complication introduced by boundary effects in small, finite networks, we only consider infinite sized networks. (Note that infinite sized networks also approximate large networks such as those envisioned for industrial control in large oil fields.)
- For grid networks, we only consider cases where the data transmission links are of equal length ℓ and ℓ is a multiple of grid hop length. We also assume a uniform traffic pattern where all the transmissions follow the same direction along the grid-line, which enables the maximum degree of spatial reuse in grid networks (the proof can be found in [19]).
- For 2D Poisson random networks, we assume that nodes are distributed with an average density of λ nodes per unit

area. The traffic pattern is such that the average link length is ℓ ; each transmitter T sends packets to a receiver R such that the distance between T and R is the closest to ℓ , and if multiple such receivers exist, T randomly picks one as its receiver.

- For both grid and random networks, we assume that each transmitter has data packets buffered for transmission with probability β at any moment in time.

The analytical results derived based on the above assumptions give us insight into the behavior of ratio-K-based scheduling in uniform grid and random networks with a wide range of system configurations (on factors such as traffic load, link length, and wireless signal attenuation); the analytical results have been verified through testbed-based measurement and simulation where finite networks and non-uniform traffic patterns are considered without the above assumptions. We will present the measurement results in Section V, and, due to space limitation, we relegate the detailed simulation results to [19].

In data transmission scheduling, we consider both reliable reception of data at receivers and reliable reception of link-layer acknowledgments at transmitters. Let the length of a link L be ℓ , and T and R be the transmitter and receiver of L respectively. Then ratio-K-based scheduling defines two circular exclusion regions centered at T and R respectively, each with a radius $K\ell$, such that no other node in the exclusion regions can transmit concurrently with T . We regard the union of the transmitter- and receiver-side exclusion regions as the exclusion region of link L , and we denote it by $\mathbb{E}\mathbb{R}(L, K)$. For instance, Figure 1 shows the exclusion region of link L in a grid network when $K = 2$. For convenience, we also use $\mathbb{E}\mathbb{R}(L, K)$ to denote the set of nodes within the exclusion region, not including those on the boundary.

Given the uniform network and traffic conditions we consider and based on the concept of *spatial throughput* [24], we define as follows the throughput T_{net} of an infinite network:²

$$T_{net} = E_L \left[\frac{T_L}{|\mathbb{E}\mathbb{R}(L, K)|} \right] \quad (4)$$

where L is an arbitrary link in the network, T_L is the throughput along link L , and $|\mathbb{E}\mathbb{R}(L, K)|$ is the number of nodes in L 's exclusion region.³ Denoting the length of L as ℓ , T_L is such that its time average can be computed as

$$E_t[T_L] = (BW \times \beta \times \text{PDR}) \times \ell \quad (5)$$

²Focusing on link-layer behavior, Sections III and IV adopt this notion of network throughput; in our measurement study in Section V, we consider end-to-end throughput which directly reflects network-wide behavior.

³We consider the expected value of $\frac{T_L}{|\mathbb{E}\mathbb{R}(L, K)|}$ to account for non-deterministic factors such as probabilistic packet transmissions and probabilistic node distribution in random networks.

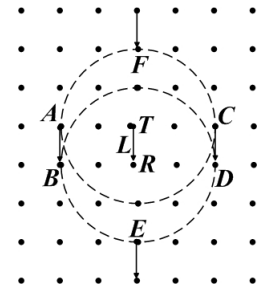


Fig. 1: Example: scheduling based on the ratio-2 model in grid networks

where BW is the radio transmission rate in terms of number of packets per unit time, β is the probability that a node has data packets buffered for transmission at any moment in time, and PDR is the packet delivery reliability over L . Note that, by the above definitions, the unit for T_L is “packet-distance-product per unit time”, and the unit for T_{net} is “packet-distance-product per unit time per node”. T_{net} characterizes the average throughput from every node to its one-hop neighbors in the network; even though T_{net} only indirectly reflects the achievable multi-hop throughput, our testbed-based measurement study in Section V will show that the insight gained in the analysis applies to the case of multi-hop convergecast. Also note that T_{net} is of direct interest to the applications of inter-vehicle sensing and control, where one typical traffic pattern is single-hop communication between neighboring vehicles.

To compute T_{net} , the key is to compute the PDR along L . Using the radio model discussed in Section II, we only need to derive the SINR value at the receiver of L in order to compute the PDR. Since it is easy to compute the reception signal strength according to Formula 1, what remains is the computation of interference at the receiver. In what follows, we present the method of computing receiver-side interference when transmissions are optimally scheduled to maximize spatial reuse without violating the ratio- K model. In the analysis, we assume that the transmission power at each transmitter is P_t .

Grid networks. The interference incurred at a receiver depends on the spatial distribution of concurrent transmitters, which depends on the specific K used in ratio- K -based scheduling. Due to space limitation, here we only present the case of $K = 2$ as shown in Figure 1; interested readers can refer to [19] for the derivation for other K s.

For the transmission along an arbitrary link L as shown in Figure 1, six nodes (i.e., $A - F$) on the boundary of the exclusion region of L can be involved, either as a transmitter or a receiver, in concurrent transmissions to generate the tightest tessellation of concurrent transmissions and to enable maximum spatial reuse. In a tightest tessellation of concurrent transmissions in ratio-2-based scheduling, this pattern of 4 concurrent transmissions/receptions around L applies to every other transmission in the network, thus we can derive the set \mathcal{S}_i of concurrent transmitters that serve as interferers to the transmission along L . If we define a coordinate system where the coordinates of R and T are $(0, 0)$ and $(0, \ell)$ respectively, then

$$\mathcal{S}_i = \{(2m\ell, (3n+1)\ell) : m \in \mathbb{Z}, n \in \mathbb{Z}, m^2 + n^2 \neq 0\} \quad (6)$$

where \mathcal{S}_i is identified by the locations of the nodes in it, and \mathbb{Z} is the set of all integers. In Figure 1, for instance, transmitter C 's location is $(2\ell, \ell)$ and the corresponding m and n are 1 and 0 respectively. Then,

Proposition 2: When $K = 2$, the expected total interference I at a receiver R in an infinite grid network is as follows:

$$I = \sum_{n_j \in \mathcal{S}_i} I_i = P_t \times \beta \times \sum_{n_i \in \mathcal{S}_i} d(n_i, R)^{-\alpha} = P_t \times \beta \times \ell^{-\alpha} \times \left(\sum_{m=1}^{\infty} \left(\frac{2}{((2m)^2+1)^{\alpha/2}} + \frac{1}{(3m+1)^{\alpha/2}} + \frac{1}{(3m-1)^{\alpha/2}} \right) + 2 \times \sum_{m=1}^{\infty} \sum_{n=1}^{\infty} \left(\frac{1}{((2m)^2+(3n+1)^2)^{\alpha/2}} + \frac{1}{((2m)^2+(3n-1)^2)^{\alpha/2}} \right) \right) \quad (7)$$

where I_i is the interference introduced by concurrent transmitter n_i , P_t is the transmission power, $d(n_i, R)$ is the distance from n_i to R , β is the node transmission probability, and α is the wireless path loss exponent. I is finite as long as $\alpha > 2$. \square (Interested readers can find the proof in [19].)

Note that, in grid networks, the total interference I is a function of link length ℓ but not the node distribution density (e.g., as characterized by the grid-hop length $\frac{\ell}{n}$ for some positive integer n).

Using Equation 7, we can compute the interference and thus the SINR at R , based on which we can compute link reliability and network throughput for the case of $K = 2$. Similar approaches can be used to derive I for other K s; interested readers can find the details in [19].

Random networks. In ratio- K -based scheduling for maximizing spatial reuse in Poisson random networks, the spatial distribution of concurrent transmitters can be modeled as a variant of the Matern hard-core process [25]. More specifically, it can be specified by a dependent thinning process as follows. Let's denote the stationary Poisson process corresponding to the random network as Φ . We mark each node X of Φ with a random number $m(X)$ uniformly distributed over $(0, 1)$; a link L with transmitter T and receiver R is marked with a number $m(L) = \frac{m(T)+m(R)}{2}$. We define the links incident to a node X as the set of links whose transmitter or receiver is X , and we denote it by $\mathbb{L}(X)$; we also denote the link whose transmitter is X by $L(X)$. Then, the dependent thinning process retains a transmitter $X \in \Phi$ if the mark of $L(X)$ is the smallest among those of all the links incident to some node within the exclusion region $\mathbb{E}\mathbb{R}(L(X), K)$ of link $L(X)$. That is, the thinned process of concurrent transmitters is defined as follows:

$$\Phi_t = \{X \in \Phi : m(L(X)) < m(L), \forall L \in \cup_{Y \in \mathbb{E}\mathbb{R}(L(X), K)} \mathbb{L}(Y)\} \quad (8)$$

Then, the thinned process Φ_t can be approximated by a spatial Poisson process [25], and we derive its density λ_t as follows:

Proposition 3: The density of the thinned process Φ_t of concurrent transmitters computes as follows:

$$\lambda_t = \frac{1 - \exp(-\lambda c)}{c} \quad (9)$$

where $c = C(\ell, K) + (C(\ell, K+1) - C(\ell, K)) \int_0^\ell \frac{2 \arccos(\frac{\ell^2 + \ell'^2 + 2K\ell\ell'}{2\ell(k\ell + \ell')})}{360\ell} d\ell'$, $C(\ell, K)$ and $C(\ell, K+1)$ is the area of the exclusion region $\mathbb{E}\mathbb{R}(L, K)$ and $\mathbb{E}\mathbb{R}(L, K+1)$ of a ℓ -long link L respectively. \square

Proof: From the results in Section 5.4 of [25], the intensity λ_t of Φ_t is given by

$$\lambda_t = p_t \lambda$$

where p_t is the *Palm retaining probability* of a 'typical point' of Φ . p_t is given by

$$p_t = \int_0^1 r(t) dt = \frac{1 - \exp(-\lambda c)}{\lambda c} \quad (10)$$

where $r(t) = \exp(-\lambda ct)$, with $c = C(\ell, K) + (C(\ell, K+1) - C(\ell, K)) \int_0^\ell \frac{2 \arccos(\frac{\ell^2 + \ell'^2 + 2K\ell\ell'}{2\ell(k\ell + \ell')})}{360\ell} d\ell'$, is the retaining probability of a node T whose associated link $L(T)$ has a mark t (i.e., $m(L(T)) = t$).

The equation for $r(t)$ follows from the observation that the point process

$$\{X \in \Phi : m(X) < t\}$$

is simply a t -thinning of the Poisson process Φ , hence itself is a Poisson process of intensity λt . Therefore, $r(t)$ is the probability that an exclusion region $\mathbb{E}\mathbb{R}(L, K + 1)$ of a ℓ -long link contains no node who has an associated link with mark less than t , that is, containing no nodes of the t -thinned process.

In computing $r(t)$, the reason why c equals $C(\ell, K) + (C(\ell, K + 1) - C(\ell, K)) \int_0^\ell \frac{2 \arccos(\frac{\ell^2 + \ell'^2 + 2K\ell\ell'}{2\ell(k\ell + \ell')})}{360\ell} d\ell'$ instead of $C(\ell, K)$ is because $\cup_{Y \in \mathbb{E}\mathbb{R}(L(X), K)} \mathbb{L}(Y)$ may well contain links whose transmitter is in $\mathbb{E}\mathbb{R}(L, K + 1)$ but not in $\mathbb{E}\mathbb{R}(L, K)$.

For a transmitter $T' \in \mathbb{E}\mathbb{R}(L, K + 1) \setminus \mathbb{E}\mathbb{R}(L, K)$ that is $K\ell + \ell'$ ($0 < \ell' \leq \ell$) from the transmitter T of link L as shown in Figure 2, the probability that T' transmits to a node in $\mathbb{E}\mathbb{R}(L, K)$ is $\frac{2\alpha}{360}$ since the receiver of T' is at any direction around T' with equal probability. Since $(K\ell)^2 = \ell^2 + (K\ell + \ell')^2 - 2\ell(K\ell + \ell')\cos\alpha$, $\alpha = \arccos(\frac{\ell^2 + \ell'^2 + 2K\ell\ell'}{2\ell(K\ell + \ell')})$.

Therefore, the probability that an arbitrary transmitter in $\mathbb{E}\mathbb{R}(L, K + 1) \setminus \mathbb{E}\mathbb{R}(L, K)$ has its receiver in $\mathbb{E}\mathbb{R}(L, K)$ is $\int_0^\ell \frac{2\alpha}{360} \frac{1}{\ell} d\ell' \int_0^\ell \frac{2 \arccos(\frac{\ell^2 + \ell'^2 + 2K\ell\ell'}{2\ell(k\ell + \ell')})}{360\ell} d\ell'$, and the expected number of nodes in $\mathbb{E}\mathbb{R}(L, K + 1) \setminus \mathbb{E}\mathbb{R}(L, K)$ whose receivers are in $\mathbb{E}\mathbb{R}(L, K)$ is $\lambda(C(\ell, K + 1) - C(\ell, K)) \int_0^\ell \frac{2 \arccos(\frac{\ell^2 + \ell'^2 + 2K\ell\ell'}{2\ell(k\ell + \ell')})}{360\ell} d\ell'$. Thus we have the formula for c .

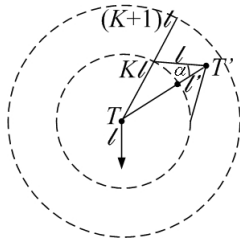


Fig. 2: Probability that a transmitter T' has its receiver in $\mathbb{E}\mathbb{R}(L, K)$

Then we can compute the total interference I at an arbitrary receiver R as follows:

Proposition 4: With ratio- K -based scheduling, the expected total interference I at a receiver R in an infinite Poisson random network is as follows:

$$I = \frac{2\pi\lambda_t P_t \beta}{(\alpha - 2)} (K\ell)^{2-\alpha} \quad (11)$$

where λ_t is given by Equation 9, P_t is the transmission power, β is the node transmission probability, α is the wireless path loss exponent, and ℓ is the link length. \square

(Interested readers can find the proof in [19].)

B. Numerical analysis

Using Formulas 4 and 5, the CC2420 radio model described in Section II, and the formulas for computing interference (e.g., Formulas 7 and 11), we numerically analyze the impact of parameter K on the network throughput and link reliability in ratio- K -based scheduling, and we analyze the impact that different network and environmental settings have on the optimal choice of parameter K .

1) *Methodology:* To examine the impact of wireless attenuation in different environments, we consider the set $\{2.1, 2.6, 3, 3.3, 3.6, 3.8, 4, 4.5, 5\}$ of wireless path loss exponents α s, which represent a wide range of real-world environments [26]; we also set the shadowing variance σ^2 based on measurement data from [26]. For the grid networks and Poisson random networks, we vary their parameters such as traffic load, link length, and node distribution density to examine the impact of network properties. Traffic load is controlled by the transmission probability β , and we consider the set $\{0.05, 0.1, 0.15, \dots, 1\}$ of β s. Link length is chosen so that the link reliability varies from 1% to 100% in the absence of interference. More specifically, for each specific path loss exponent α , we choose a link length ℓ_0 corresponding to an interference-free packet delivery rate (PDR) of 1%, and another link length ℓ_1 corresponding to a signal-to-noise-ratio (SNR) of 5dB more than the minimum SNR for ensuring 100% interference-free PDR; then we take 60 sample link lengths that are uniformly distributed between ℓ_0 and ℓ_1 . (Note that the transmission power level is set at -25dBm in our study.) For each average link length ℓ in random networks, we select a set of node distribution densities λ s so that the average number of nodes in a circular area of radius ℓ is 5, 10, 15, 20, 30, and 40 respectively.

For convenience, we regard each setting of network and environment parameters as a *system configuration* hereafter. Thus our study examines 75,600 different system configurations, and the boxplots, medians, and distributions to be presented in the rest of the paper are mostly based on the distribution of the corresponding metrics across different system configurations. For each system configuration, we analyze the network performance when the ratio- K model is instantiated with different K s. The set of K s we consider are $\{\sqrt{2}, 2, \sqrt{5}, \sqrt{8}, 3, \sqrt{10}, \sqrt{13}, 4, \sqrt{18}, \sqrt{20}, 5, \sqrt{26}, \sqrt{29}, \sqrt{34}, 6\}$ ⁴ for grid networks, and $\{1, 1.5, 2, 2.5, \dots, 10\}$ for Poisson random networks. Using the numerical results on network throughput and link reliability in these 75,600 system configurations, we analyze 1) the impact of different factors on the best ratio- K model instantiation, 2) the sensitivity of model instantiation, and 3) the tradeoff between reliability and throughput in instantiating the ratio- K model. *The observations in grid networks and random networks are similar; thus here we only present results for grid networks; detailed results for random networks can be found in [19].*

2) *Sensitivity of ratio- K -based scheduling:* We have analyzed how different network and environmental factors affect the optimal K that maximizes network throughput and the minimum K for ensuring certain link packet delivery rate (PDR). We have found that network and environmental properties significantly affect the best instantiation of the ratio- K model. Due to the limitation of space, we relegate the detailed discussion to [19]; but to illustrate the drawbacks of choosing a constant K for ratio- K -based scheduling as in most existing study, we present in what follows the summary results on

⁴These K s are chosen in a *continuous* manner in the sense that, given a receiver, the inner area enclosed by the boundaries of the exclusion regions associated with every two closest K s does not contain any node. We find that, for ratio- K -based scheduling in grid networks, increasing K after K is already greater than 5 can only increase link reliability but not network throughput. Thus 6 is large enough to serve as the largest K in our study.

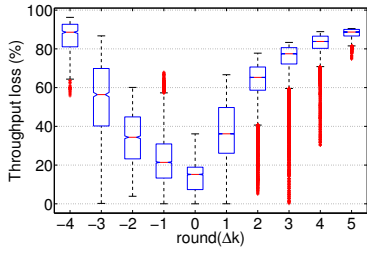


Fig. 3: Throughput loss when using $K = K_{opt} + \Delta K$

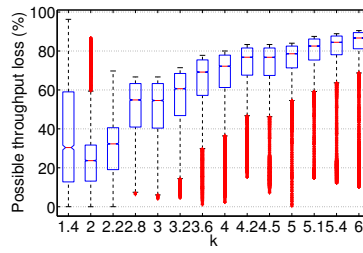


Fig. 4: Possible throughput loss by choosing a constant K

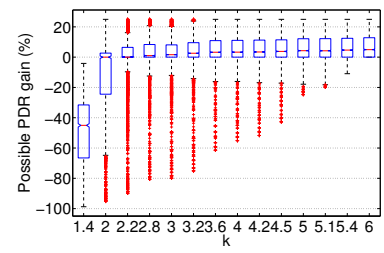


Fig. 5: Impact of using a constant K: PDR req. = 80%

the sensitivity of network throughput and link reliability with respect to network and environmental dynamics.

Throughput. Given that the optimal K for maximizing network throughput changes with network and environmental properties, using any constant K in ratio- K -based scheduling may lead to throughput loss since the chosen K may not always be optimal. To quantify the impact of not adapting K to network and environmental dynamics, we compute, for each system configuration, the loss in network throughput when using a K that is ΔK away from the optimal K , denoted by K_{opt} , for this system configuration. For different ΔK 's, Figure 3 shows the boxplot⁵ of throughput loss across different system configurations, where the loss is defined as the reduction in throughput divided by the optimal throughput. We see that, in general, throughput loss increases as $|\Delta K|$ increases. If the used K differs from the optimal one by up to 1, throughput loss can be up to 68%, which is non-negligible.

To understand the impact of choosing a fixed K , Figure 4 shows, for different fixed K s, the possible throughput loss across different system configurations. We see that the throughput loss can be significant. For instance, fixing K to 2 can lead to a throughput loss of up to 86.73% and a median loss of 23.68%.

Therefore, using a constant K across different network and environmental settings may well lead to significant loss in network throughput, and, to avoid biased evaluation against ratio- K -based scheduling, we need to take this into account in both protocol design and performance analysis.

Reliability. To understand the impact of using a constant K on link reliability, we consider system configurations where a proper choice of K can ensure a link reliability of at least 20%, 40%, 60%, 80%, and 100%. Due to the limitation of space, here we only present the data for configurations where a link reliability of at least 80% can be achieved by choosing a proper K . (Similar phenomena as what we will present have been observed for other configurations too.) Figure 5 shows, for using different K s, the boxplot of the PDR (i.e., packet delivery rate) gain across different system configurations, where the PDR gain is defined as $\frac{\text{PDR}_k - 0.8}{0.8}$ and PDR_k is the PDR resulting from using a specific constant K in a system configuration.

We see that K s less than or equal to 2 tend not to be a good constant number for ensuring reliable data delivery (e.g., 80% link PDR): a constant K of 2 is unable to guarantee

80% link reliability with non-negligible probability; a constant K of $\sqrt{2}$ is mostly unlikely to guarantee 80% reliability, even though $\sqrt{2}$ is the optimal K for maximizing throughput in a wide variety of system configurations we study. On the other hand, using larger K s (e.g., 4) can improve link reliability, but this usually comes at the cost of reduced network throughput due to reduced spatial reuse of channel resources (as can be seen from Figure 4). We study this tradeoff between reliability and throughput in detail next.

3) *Tradeoff between reliability and throughput:* The above discussion has alluded to the inherent tradeoff between link reliability and network throughput in instantiating the ratio- K model. In what follows, we examine the issue in detail.⁶ For each link reliability requirement (e.g., 80%) and each system configuration that can ensure the reliability by using certain minimum $K = K_0$, we compute the performance gain in packet delivery rate (PDR) and throughput when changing K to $K' = (K_0 + \Delta K)$ for various ΔK 's. The performance gain is defined as $\frac{X_{K'} - X_0}{X_0}$, where X_0 is the PDR (or throughput) when $K = K_0$ and $X_{K'}$ is the PDR (or throughput) when $K = K'$.

Figure 6 shows the median performance gains for system configurations where a certain minimum PDR can be ensured, and we observe the following: 1) *maximum network throughput is usually not achieved at the minimum K for ensuring certain link reliability but at a smaller K* ; 2) *as K increases from the minimum one for ensuring certain link reliability, network throughput tends to decrease with high probability even though link reliability does improve*; 3) *as PDR requirement increases, moreover, the probability of improving throughput by increasing K from the minimum one of ensuring the PDR requirement further decreases, in addition to being small all the time.*

Implications. These findings suggest that we should use, in protocol design, the minimum K that ensures the required link reliability, since this helps avoid throughput reduction while ensuring enough reliability at the same time. In general, the minimum link reliability required is application dependent, and it relates to the question of how to balance properties such as throughput, reliability, delay, and energy efficiency. In low-power wireless sensing and control networks such as those for industrial sensing and control, however, it is usually desirable to have high link reliability for the following reasons: 1) reliable data delivery itself is usually important for mission-critical sensing and control; 2) higher reliability implies less

⁵Note that, for clarity of presentation, we group data by the rounded ΔK instead of ΔK directly because there are too many ΔK 's to present individually in a single figure.

⁶We numerically study the tradeoff because it is difficult to derive the closed-form formula for the relationship between link reliability and network throughput in general.

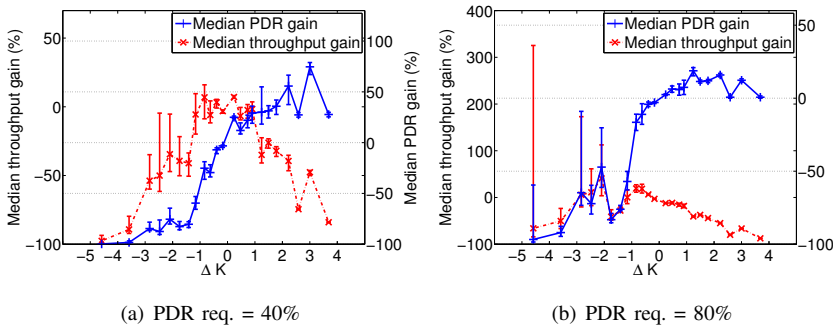


Fig. 6: Δk vs. performance gain

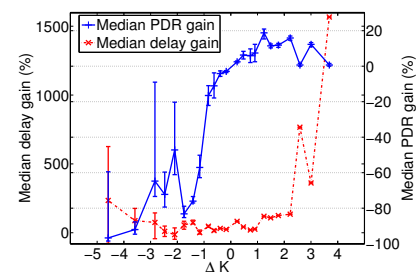


Fig. 7: Δk vs. delay increase: TDMA, PDR req. = 80%

variability and better predictability in data delivery performance (e.g., timeliness); this is because, given a link reliability p , the coefficient-of-variation of packet transmission status (i.e., success or failure) is $\sqrt{\frac{1-p}{p}}$ which decreases as p increases; 3) higher reliability implies fewer number of packet retransmissions and thus less energy consumption. Given that, for high reliability requirement, the probability of throughput loss is high when we increase K beyond the minimum one required for ensuring reliability, PDR requirement can serve as a good basis for a node to choose the right K to use.

Choosing the minimum K that ensures the required link reliability also tends to help reduce data delivery delay. For grid networks with TDMA channel access control, for instance, Figure 7 shows the highly-likely increase in one-hop data delivery delay as K deviates, by ΔK , from the minimum one K' that ensures a required link reliability. (Interested readers can find the delay analysis in [19].) As K increases from K' , the delay increases because the number of nodes in a link's exclusion region increases, which introduces larger contention delay in channel access. As K decreases from K' , the contention delay decreases, but the overall delay still tends to increase because retransmissions are required to ensure the same link-layer data delivery reliability as what is enabled by K' without retransmission. Similar phenomena are observed for random networks and TDMA channel access control mechanisms [19]. Given that the performance (e.g., convergence rate) of networked control usually decreases dramatically with increasing network delay, it is important to ensure small network delay in mission-critical sensing and control, which further emphasizes the need for high link reliability.

C. Summary and the PRK interference model

Through detailed study with different configurations of grid and random networks, we find that both network throughput and link reliability are sensitive to the choice of K in instantiating the ratio- K model. Thus it is important to take this into account in both protocol design and performance evaluation, for instance, by adapting K to network and environmental dynamics in protocol design and by using the optimal K for quantifying achievable performance in ratio- K -based scheduling.

We also observe that there is inherent tradeoff between link reliability and network throughput. In ratio- K -based scheduling, therefore, it is desirable to use the minimum K that ensures the required link reliability, since this tends to avoid throughput loss

caused by using any unnecessarily large K . This observation suggests that link reliability requirement can serve as a good basis for each node to choose the right K to use in ratio- K -based scheduling. Accordingly, we propose the *physical-ratio- K* (PRK) interference model as a link-reliability-based instantiation of the ratio- K model as follows: “Given a transmission from node n_s to node n_r , a concurrent transmitter n_i does not interfere with the reception at n_r if and only if the following holds:

$$P(n_i, n_r) < \frac{P(n_s, n_r)}{K_{n_s, n_r, T_{pdr}}} \quad (12)$$

where $P(n_i, n_r)$ and $P(n_s, n_r)$ is the strength of signals reaching n_r from n_i and n_s respectively, and $K_{n_s, n_r, T_{pdr}}$ is chosen such that the probability of n_r successfully receiving packets from n_s is at least T_{pdr} in the presence of interference from all concurrent transmitters.” It is usually difficult to derive closed-form formula for computing the parameter $K_{n_s, n_r, T_{pdr}}$ in general. But K is amenable to online, distributed instantiation, because link reliability is a locally measurable metric and can even be identified through real-time, data-driven, passive measurement [6]. In particular, the problem of identifying parameter $K_{n_s, n_r, T_{pdr}}$ can be modeled as a classical “regulation control” problem [27], where the “reference input” is the required link reliability T_{pdr} , the “control input” is the parameter $K_{n_s, n_r, T_{pdr}}$, and the “feedback” is the current link reliability from n_s to n_r . Because the adaptation of K is local and the signal strength between nearby nodes is a pairwise, locally measurable metric too, we expect the PRK model to be a good basis for designing distributed MAC protocols. Since our focus in this paper is understanding behavior of ratio- K -based scheduling instead of protocol design, we relegate the study of distributed, PRK-based medium access control to our future work. But we will study the potential performance of PRK-based medium access control in Section IV.

Based on the above discussion, we see that the PRK model has the locality of the ratio- K model. The PRK model also has the high fidelity of the SINR model, since it is based on link reliability which captures the properties and constraints of wireless communication. Even though the parameter $K_{n_s, n_r, T_{pdr}}$ of the PRK model depends on interference from all concurrent transmitters in the network as in the SINR model, the PRK model is simpler than the SINR model in terms of distributed protocol design. This is because, unlike the SINR model which *explicitly* characterizes interference from each concurrent trans-

mitter in the whole network, interference is modeled *implicitly* in the PRK model through locally measurable link reliability without worrying about who the concurrent transmitters are. Thus, the PRK model enables a receiver to locally adapt the parameter K for satisfying its local link reliability requirement without explicit network-wide coordination.

We define the PRK model based on signal strength instead of geographic distance so that the model is more generically applicable, for instance, to scenarios where transmission power varies across nodes [17] or signal attenuation is non-uniform such as in our measurement study of Section V. Note that the selection of $K_{n_s, n_r, T_{pdr}}$ is based on each link of a receiver n_r such that the model can also be applied to cases where different links of a receiver vary significantly, for instance, in their senders' transmission powers. To relate the PRK model to the ratio-K model and to facilitate discussions in Sections IV and V, we define the concept *s-distance* as follows: the *s-distance* from a node T to another node R , denoted by $sd(T, R)$, is $\frac{1}{P(T, R)}$ where $P(T, R)$ is the strength of signals reaching R from T . If $sd(T_1, R) > sd(T_2, R)$, then T_1 is regarded as *s-farther* away from R than T_2 is, and T_2 is regarded as *s-closer* to R than T_1 is. Given a $K' = K_{n_s, n_r, T_{pdr}}$, the PRK model defines an exclusion region $\mathbb{E}\mathbb{R}(n_r, K')$ around the receiver n_r such that a node n_j is in $\mathbb{E}\mathbb{R}(n_r, K')$ if and only if $sd(n_j, n_r) < \mathbb{R}(n_s, n_r, K')$, where $\mathbb{R}(n_s, n_r, K') = \frac{K'}{P(n_s, n_r)}$ is called the *s-radius* of the exclusion region $\mathbb{E}\mathbb{R}(n_r, K')$.

IV. OPTIMALITY OF PRK-BASED SCHEDULING

While detailed study of distributed protocol design using the PRK model is a part of our future work, we analyze in this section the optimality of PRK-based scheduling as compared with SINR-based scheduling to gain insight into the potential effectiveness of PRK-based scheduling.⁷ For ensuring data delivery reliability in wireless networked sensing and control, we conduct our comparative analysis on the condition that the link reliability in PRK- and SINR-based scheduling be the same.

A. Throughput loss in PRK-based scheduling

Similar to Section III-A, our analysis here considers infinite sized grid and Poisson random networks with uniform traffic patterns. We will verify the analytical results through testbed-based measurement (see Section V) and simulation (see [19]) where finite networks and non-uniform traffic patterns are considered.

To satisfy a certain link reliability requirement and thus a certain packet-delivery-rate (PDR) for data and acknowledgment (ACK) reception along a link L , we need to make sure that the SINR at the receiver R and the transmitter T is above a certain threshold γ_0 and γ'_0 respectively. For a given received signal strength P_r and background noise N_0 at R , this requirement translates into a requirement on controlling the maximum interference I_t at R to be $\frac{P_r}{\gamma_0} - N_0$. Similarly, we can

⁷Here we do not perform detailed comparative study between PRK- and ratio-K-based scheduling because it is obvious from Section III that, by adapting to network and environmental conditions as well as application requirements, PRK-based scheduling will perform better than ratio-K-based scheduling.

derive the maximum tolerable interference I'_t at T .⁸ To control interference, we need to silence the transmission of some nodes in the network, and to maximize network spatial throughput, we need to minimize the number of silenced transmitters. To this end, we have

Proposition 5: To minimize the number of nodes silenced for ensuring certain minimum SINR at the receiver R (or the transmitter T) in both PRK- and SINR-based scheduling, nodes *s-closer* to R (or T) rather than those *s-farther* away should be silenced first. \square

(Interested readers can find the proof in [19].)

Therefore, the set \mathcal{S} of nodes silenced by the data reception at receiver R are the $|\mathcal{S}|$ number of nodes *s-closest* to R , where $|\mathcal{S}|$ denotes the cardinality of set \mathcal{S} . We denote the set of nodes silenced by R in SINR- and PRK-based scheduling as \mathcal{S}_{sinr} and \mathcal{S}_{prk} respectively. For a tolerable interference I_t at R , we let I_{sinr} and I_{prk} be the actual interference incurred at R in SINR- and PRK-based scheduling respectively. Similarly, for correct ACK reception at the transmitter T in SINR- and PRK-based scheduling, we denote the set of silenced nodes as \mathcal{S}'_{sinr} and \mathcal{S}'_{prk} respectively, and, for a tolerable interference I'_t at T , we let I'_{sinr} and I'_{prk} be the actual interference incurred at T respectively. We also define $\mathbb{S}_{sinr} = \mathcal{S}_{sinr} \cup \mathcal{S}'_{sinr}$ and $\mathbb{S}_{prk} = \mathcal{S}_{prk} \cup \mathcal{S}'_{prk}$ to represent the set of silenced nodes around link L in SINR- and PRK-based scheduling respectively. Then,

Proposition 6: Given the tolerable interference I_t and I'_t at the receiver R and the transmitter T respectively, $\mathbb{S}_{sinr} \subseteq \mathbb{S}_{prk}$, $I_{prk} \leq I_{sinr} \leq I_t$, and $I'_{prk} \leq I'_{sinr} \leq I'_t$. \square

Proof: Let the longest *s-distance* from a node in \mathcal{S}_{sinr} to R be d_{sinr} . By the definition of the PRK and the SINR models and Proposition 5, all the nodes in \mathcal{S}_{sinr} and \mathcal{S}_{prk} are within d_{sinr} *s-distance* away from the receiver R . The difference between the PRK model and the SINR model is that, by the definition of the PRK model (see Inequality 12), all the nodes that are d_{sinr} *s-distance* away from R have to be silenced in the PRK model as long as at least one of them has to be silenced; whereas in the SINR model, we only need to silence the minimum number of nodes d_{sinr} *s-distance* away from R to ensure that the SINR at R is at least γ_0 . For example, in Figure 8, there are four nodes d_{sinr} *s-distance* away from R . While the SINR model may only need to silence node A to guarantee the SINR threshold I_t , the PRK model will silence all the four nodes d_{sinr} away. Therefore, $\mathcal{S}_{sinr} \subseteq \mathcal{S}_{prk}$. Since $\mathcal{S}_{sinr} \subseteq \mathcal{S}_{prk}$, $I_{prk} \leq I_{sinr}$. SINR-based scheduling will ensure that $I_{sinr} \leq I_t$. Thus, $I_{prk} \leq I_{sinr} \leq I_t$ holds.

Similar argument applies to the transmitter T . Thus, $\mathcal{S}'_{sinr} \subseteq$

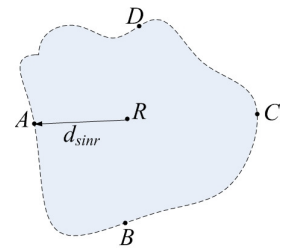


Fig. 8: Difference in PRK- and SINR-based scheduling: receiver oriented view

⁸ I'_t may or may not equal to I_t depending on the ACK mechanism and the wireless radios. Accordingly, the exclusion regions around the sender and the receiver of a transmission may or may not be the same in PRK-based scheduling.

\mathcal{S}'_{prk} , and $I'_{prk} \leq I'_{sindr} \leq I'_t$. Since $\mathcal{S}_{sindr} \subseteq \mathcal{S}_{prk}$ and $\mathcal{S}'_{sindr} \subseteq \mathcal{S}'_{prk}$, $\mathbb{S}_{sindr} \subseteq \mathbb{S}_{prk}$. ■

Now, we are ready to derive the upper bound on the throughput loss in PRK-based scheduling as compared with SINR-based scheduling. By Formulas 4 and 5, the throughput of PRK- and SINR-based scheduling, denoted by T_{prk} and T_{sindr} respectively, can be computed as follows:

$$T_{prk} = \frac{T_{R,prk}}{|\mathbb{S}_{prk}|} \quad T_{sindr} = \frac{T_{R,sindr}}{|\mathbb{S}_{sindr}|}$$

where $T_{R,prk}$ and $T_{R,sindr}$ are the link throughput to R in PRK- and SINR-based scheduling respectively. From Proposition 6, we know that the average link reliability in SINR-based scheduling is no higher than that in PRK-based scheduling (since the actual interference incurred in SINR-based scheduling is no less than that in PRK-based scheduling). Thus, $T_{R,sindr} \leq T_{R,prk}$. Then, we can define the throughput loss T_{loss} in PRK-based scheduling as

$$\begin{aligned} T_{loss} &= \frac{T_{sindr} - T_{prk}}{T_{sindr}} = \frac{\frac{T_{R,sindr}}{|\mathbb{S}_{sindr}|} - \frac{T_{R,prk}}{|\mathbb{S}_{prk}|}}{\frac{T_{R,sindr}}{|\mathbb{S}_{sindr}|}} \\ &\leq \frac{\frac{T_{R,sindr}}{|\mathbb{S}_{sindr}|} - \frac{T_{R,prk}}{|\mathbb{S}_{prk}|}}{\frac{T_{R,sindr}}{|\mathbb{S}_{sindr}|}} = \frac{|\mathbb{S}_{prk}| - |\mathbb{S}_{sindr}|}{|\mathbb{S}_{prk}|} \end{aligned} \quad (13)$$

Let n_b be the node in \mathcal{S}_{sindr} that is s-farthest away from the receiver R , P_0 be the power of signals that reach R from n_b , and N_b be the number of nodes in the network whose s-distance to R is $sd(n_b, R)$. Similarly, let n'_b be the node in \mathcal{S}'_{sindr} that is s-farthest away from the transmitter T , P'_0 be the power of signals that reach T from n'_b , and N'_b be the number of nodes whose s-distance to T is $sd(n'_b, T)$. Then,

Proposition 7: The expected T_{loss} is less than or equal to $\frac{1}{|\mathbb{S}_{prk}|} (\min\{\frac{I_t - I_{prk}}{P_0 \times \beta}, N_b\} + \min\{\frac{I'_t - I'_{prk}}{P'_0 \times \beta}, N'_b\})$. □

Proof: Let $dist(n_b, R)$ be the s-distance from n_b to R , and $dist(n'_b, T)$ be the s-distance from n'_b to T . Then from the proof of Proposition 6, we know that the s-distance d from every node in $\mathcal{S}_{prk} \setminus \mathcal{S}_{sindr}$ to R is $dist(n_b, R)$ since the PRK model silences all the nodes on the boundary of the exclusion region around R . Similarly, the s-distance d' from every node in $\mathcal{S}'_{prk} \setminus \mathcal{S}'_{sindr}$ to T is $dist(n'_b, T)$.

Given the interference tolerance I_t and I'_t at R and T respectively, the set of silenced nodes \mathbb{S}_{prk} is fixed for a tightest tessellation of concurrent transmitters in a specific network and environmental setting. To understand the upper bound on T_{loss} , we need to understand the upper bound on $(|\mathbb{S}_{prk}| - |\mathbb{S}_{sindr}|)$ (see Inequality 13). By the definition of \mathbb{S}_{prk} and \mathbb{S}_{sindr} , we know that $|\mathbb{S}_{prk}| - |\mathbb{S}_{sindr}| \leq (|\mathcal{S}_{prk}| - |\mathcal{S}_{sindr}|) + (|\mathcal{S}'_{prk}| - |\mathcal{S}'_{sindr}|)$. To upper bound $(|\mathbb{S}_{prk}| - |\mathbb{S}_{sindr}|)$, we analyze in what follows the upper bound on $(|\mathcal{S}_{prk}| - |\mathcal{S}_{sindr}|)$ and $(|\mathcal{S}'_{prk}| - |\mathcal{S}'_{sindr}|)$.

We first derive the upper bound on $(|\mathcal{S}_{prk}| - |\mathcal{S}_{sindr}|)$. Since all the nodes in $\mathcal{S}_{prk} \setminus \mathcal{S}_{sindr}$ are on the boundary of the exclusion region around R and are $dist(n_b, R)$ s-distance away from R , each such node introduces an expected interference of $P_0 \times \beta$ at receiver R . To ensure that the expected interference at R is no more than I_t (a.k.a., the SINR at R is above γ_0), one necessary condition is that the expected interference introduced by nodes in $\mathcal{S}_{prk} \setminus \mathcal{S}_{sindr}$ should be no more than $I_t - I_{prk}$, that is, the number of nodes in $\mathcal{S}_{prk} \setminus \mathcal{S}_{sindr}$ should be no more than $\frac{I_t - I_{prk}}{P_0 \times \beta}$. Note that this upper bound is usually not tight and

not a sufficient condition because the interference at R tends to exceed I_t if the interferences from nodes in $\mathcal{S}_{prk} \setminus \mathcal{S}_{sindr}$ reaches $I_t - I_{prk}$. This is because, if we add, for every area of the same size of the exclusion region around R , $\frac{I_t - I_{prk}}{P_0 \times \beta}$ more transmitters on average in SINR-based scheduling than in PRK-based scheduling, the interference at R will exceed $I_t - I_{prk}$ when the area covered by the network is larger than the exclusion region around R (which is usually the case). Therefore, an upper bound on the number of nodes in $\mathcal{S}_{prk} \setminus \mathcal{S}_{sindr}$ is $\frac{I_t - I_{prk}}{P_0 \times \beta}$. In addition, the number of nodes on the boundary of the exclusion region around R is no more than N_b , thus $(|\mathcal{S}_{prk}| - |\mathcal{S}_{sindr}|) \leq \min\{\frac{I_t - I_{prk}}{P_0 \times \beta}, N_b\}$.

Similarly, we can derive that $(|\mathcal{S}'_{prk}| - |\mathcal{S}'_{sindr}|) \leq \min\{\frac{I'_t - I'_{prk}}{P'_0 \times \beta}, N'_b\}$. Putting the above analysis together, the expected T_{loss} is no more than $\frac{1}{|\mathbb{S}_{prk}|} (\frac{I_t - I_{prk}}{P_0 \times \beta} + \frac{I'_t - I'_{prk}}{P'_0 \times \beta})$. ■

Proposition 7 enables us to compute the upper bound, denoted by T_{lb} , on the throughput loss in PRK-based scheduling. For convenience, we let $\Delta X = \min\{\frac{I_t - I_{prk}}{P_0 \times \beta}, N_b\} + \min\{\frac{I'_t - I'_{prk}}{P'_0 \times \beta}, N'_b\}$, and thus $T_{lb} = \frac{\Delta X}{|\mathbb{S}_{prk}|}$. Note that ΔX represents an upper bound on $|\mathcal{S}_{prk} \setminus \mathcal{S}_{sindr}|$, that is, the average number of nodes per exclusion region that are silenced in PRK-based scheduling but not in SINR-based scheduling. In the next subsection, we numerically analyze the properties of ΔX and T_{lb} .

B. Numerical analysis

Using the same network and environmental settings of Section III-B1 and based on Proposition 7, we analyze the throughput loss in PRK-based scheduling as compared with SINR-based scheduling. For each of the system configurations we study, more specifically, we first find I_t , I'_t , and the minimum K value of the PRK model for satisfying certain link reliability requirement, then we compute $|\mathbb{S}_{prk}|$, I_{prk} , and I'_{prk} which in turn enable us to compute ΔX and T_{lb} according to Proposition 7.

Grid networks. For each system configuration, we compute the ΔX and throughput loss in PRK-based scheduling. For different requirements on packet delivery rate (PDR), Figure 9 shows the boxplot of throughput loss in PRK-based scheduling in different system configurations. We see that *the throughput loss is small in general, and it also tends to decrease as the PDR requirement increases*. For instance, the median throughput loss is less than 5% when the required PDR is 50%, and the median throughput loss is less than 1% when the required PDR is 90%. These findings imply that, for mission-critical wireless networking where the PDR requirement is usually high, PRK-based scheduling can enable a performance very close to what is possible with SINR-based scheduling.

The reason why throughput loss is low in the PRK model is because ΔX tends to be small. For instance, ΔX is less than 1 in more than 99% of the system configurations we study.

Random networks. Table I shows the median throughput loss for different λ 's and PDR requirements. We see that, similar to grid networks, throughput loss decreases as PDR requirement increases. Moreover, we see that throughput loss also decreases as node distribution density λ increases, and this is because

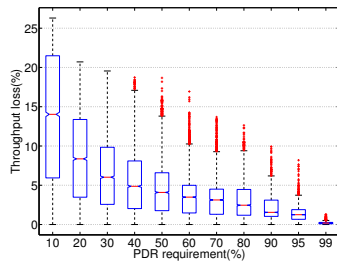


Fig. 9: Throughput loss in PRK-based scheduling: grid networks



Fig. 10: *NetEye* wireless sensor network testbed

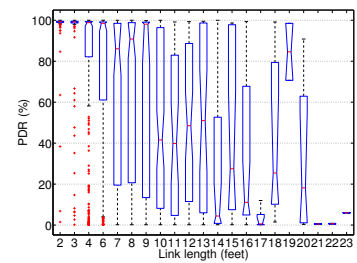


Fig. 11: PDR vs. link length in *NetEye* when transmission power is -25dBm

PDR req. (%)	20	40	60	80	99
$\lambda = 3.18$	8.87	7.01	6.25	5.21	4.20
$\lambda = 6.37$	7.60	6.01	5.36	4.46	3.60
$\lambda = 9.55$	6.65	5.26	4.69	3.91	3.15
$\lambda = 12.74$	5.91	4.68	4.17	3.47	2.80

TABLE I: Impact of λ and PDR requirement on median throughput loss (%)

larger λ increases the number of silenced nodes in the PRK model (i.e., $|\mathbb{S}_{prk}|$) at a faster rate than the corresponding increase in ΔX .

Summary. Our findings suggest that PRK-based scheduling can perform very well compared with SINR-based scheduling: PRK-based scheduling enables a network throughput very close to what is possible in SINR-based scheduling while ensuring the same required PDR. The performance of PRK-based scheduling also improves as the PDR requirement increases, which implies that PRK-based scheduling can perform well in mission critical wireless networks such as those for real-time, reliable sensing and control.

V. MEASUREMENT STUDY OF PRK- AND SINR-BASED SCHEDULING

Our analytical results show that the PRK model serves well as the basis of instantiating the ratio-K model in different network and environmental settings and that PRK-based scheduling achieves a spatial throughput close to what is possible in SINR-based scheduling. To corroborate these results, we experimentally compare the performance of PRK- and SINR-based scheduling using the *NetEye* wireless sensor network testbed [28] at Wayne State University and the *MoteLab* testbed [29] at Harvard University, and we also experimentally verify the tradeoff between reliability and throughput in both PRK- and SINR-based scheduling. To reflect the impact of link-layer behavior on network-wide behavior, we also consider end-to-end throughput in this section. The purposes of this measurement evaluation are to verify the analytical results and to correct the misconceptions about the potential performance of ratio-K-based scheduling, thus our evaluation will be based on the centralized scheduling algorithm Longest-Queue-First (LQF) that has been used to compare different wireless interference models by Maheshwari et al. [9]. Distributed protocol design via the PRK model is a part of our future work.

A. Methodology

We use both the *NetEye* and the *MoteLab* testbeds so that we can evaluate PRK- and SINR-based scheduling in different network and environmental settings. In what follows, we first describe properties of the two testbeds, then we discuss the traffic patterns and the scheduling objectives studies here.

NetEye testbed. *NetEye* [28] is deployed in an indoor office as shown in Figure 10. We use a 10×12 grid of TelosB motes in *NetEye*, where every two closest neighboring motes are separated by 2 feet. Each of these TelosB motes is equipped with a 3dB signal attenuator and a 2.45GHz monopole antenna. In our measurement study, we set the radio transmission power to be -25dBm (a.k.a. power level 3 in TinyOS) such that multihop networks can be created. In addition to grid networks, the 10×12 grid enables us to experiment with random networks, where a random network is generated out of the 10×12 grid by removing each mote of the grid with certain probability.

Part of the input to PRK- and SINR-based scheduling algorithms (to be discussed in Section V-B) are radio model, background noise at every node, and strength of signals from any one node to every other node. To collect these information about the 10×12 grid in *NetEye*, we perform the following experiment: let the 120 motes take turns to be a transmitter one at a time; when a mote is a transmitter, it broadcasts 600 128-byte packets with a transmission power of -25dBm and an inter-packet interval of 100ms (note: each packet transmission takes ~ 4 ms); while a mote is transmitting packets, every other mote keeps sampling its radio RSSI once every 2ms whether or not it can receive packets from the transmitter, and, if a mote can receive packets from the transmitter, it logs the received packets. Using the data collected in this experiment, we can derive the background noise power at each node,⁹ the strength of signals from any node to every other node, and the packet delivery rate (PDR) from any node to every other node as well as the associated SINR. These data also enable us to derive the empirical radio model for the TelosB motes in *NetEye*, and the radio model shows the relation between PDR and SINR. We will use this radio model in our scheduling algorithms for two purposes: 1) to choose the SINR threshold for satisfying certain link reliability, and 2) to compute the expected PDR for a given SINR at a receiver. For the transmission power of -25dBm, Figure 11 shows the boxplot of PDR for links of different length, and Figure 12 shows the histogram of

⁹It is derived from RSSI readings in the absence of packet transmission.

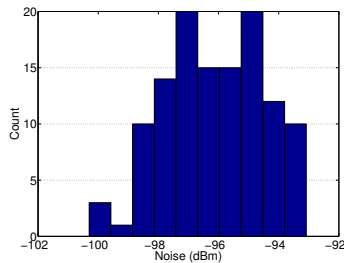


Fig. 12: Histogram of background noise power in NetEye

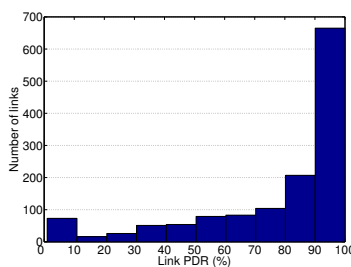


Fig. 13: Histogram of link PDRs in MoteLab

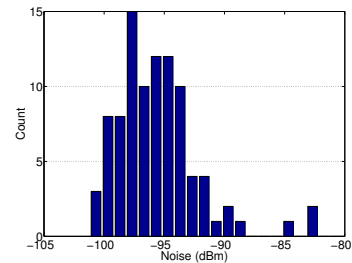


Fig. 14: Histogram of background noise power in MoteLab

background noise power in NetEye. We see that there is a high degree of variability in PDR for links of equal length and in background noise power. Thus the testbed enables us to do experiments in non-uniform settings.

MoteLab testbed. MoteLab is deployed at three floors of the EECS building of Harvard. Our experiments use all of the 101 operational Tmote Sky motes, with 32, 39, and 30 motes distributed at the first, second, and third floors respectively. We use a transmission power of -1dBm (a.k.a. power level 27) to generate a well-connected multi-hop networks.

Using a method similar to that for NetEye, we have characterized the empirical radio model, background noise at every node, and strength of signals from any node to every other node in MoteLab. Figure 13 shows the histograms of the PDRs of all the wireless links, and Figure 14 shows the histogram of background noise power in MoteLab. We see that there is a high degree of variability in link PDRs and background noise power. Thus the testbed enables us to do experiments in non-uniform settings too.

Traffic patterns. To generate the traffic load for scheduling, we consider convergecast in wireless sensor networks where data packets generated by all the nodes need to be delivered to a base station node.

For NetEye, we consider convergecast in both grid and random networks. For grid network, we let the node at one corner serve as the base station to which the remaining nodes of the 10×12 grid deliver their packets (mostly via multi-hop paths); we generate the random network out of the 10×12 grid by removing a mote in the grid with 30% probability, and then we let a mote closest to a corner of the original grid be the base station (with ties broken randomly). In both the grid and random networks, an approximate routing tree is built by letting each mote choose as its parent the mote having the minimum ETX (i.e., expected transmission count) value to the base station among all the motes within 6 feet distance. Given a routing tree, we generate the traffic load as follows: each node generates a packet with 50% probability, and then the number of packets that need to be delivered across a link is the number of packets generated in the subtree rooted at the transmitter of the link. Then the traffic load is used as the input to PRK- and SINR-based scheduling. (Note that this traffic load can simulate event detection and may also be repeated to simulate periodic data collection in sensor networks.)

For MoteLab, we let mote #115 at the center of the second floor be the base station to which the remaining 100 motes

deliver their packets (mostly via multi-hop paths). Then the routing tree and network traffic are generated in the same manner as in NetEye.

Scheduling objectives. When scheduling the aforementioned traffic load, we consider three different scheduling objectives: 1) *Obj-5*: to guarantee a 5dB minimum SINR at transmitters and receivers (with throughput maximization as a second-order objective), which corresponds to a link PDR of $\sim 88\%$ and $\sim 97\%$ in NetEye and MoteLab respectively; 2) *Obj-8*: to guarantee an 8dB minimum SINR at transmitters and receivers, which corresponds to a link PDR of $\sim 95\%$ and $\sim 98\%$ in NetEye and MoteLab respectively; and 3) *Obj-T*: to maximize network throughput. When comparing PRK- and SINR-based scheduling for different objectives and networks, we consider both link PDR and network throughput.

Overall, we have 12 different experiment configurations, where each configuration specifies a scheduling objective, a topology, and an interference model. A schedule is generated by our scheduling algorithms for each system configuration, where the schedule $S = \{S_1, S_2, \dots, S_\tau\}$, with S_j being a set of links scheduled in j -th time slot and τ being the schedule length. Experiment with each schedule is repeated 10 times to gain statistical insight. To experiment with a schedule in NetEye, we select a mote not in the 10×12 grid to be the commander that broadcasts the schedule, slot by slot, to the motes involved (as either a transmitter or a receiver) in each slot such that the links in the same slot are synchronized to transmit at the same time; each slot is repeated 30 times before moving onto the next slot so that we can get 30 samples on the transmission status (i.e., success or failure) along each link of the slot to understand the behavior of each slot.

In the next subsection, we describe the scheduling algorithms used in our evaluation.

B. Scheduling algorithms

Optimal SINR- and ratio-K-based scheduling are NP-complete in general [16], [8], thus we use the greedy, approximate scheduling framework, denoted by Longest-Queue-First (LQF) [30], [31], [32],¹⁰ that has been used to compare differ-

¹⁰Note that the LQF scheduling framework has been shown to achieve close-to-optimal throughput in many practical scenarios [30], [31] and has been a research focus in recent years. Besides LQF, we have also experimented with other scheduling algorithms such as the commonly-used GreedyPhysical [33], [34] and the recently proposed iOrder [35] algorithm. Similar phenomena have been observed for different algorithms, and here we only present the results based on LQF due to the limitation of space; interested readers can find the results based on GreedyPhysical and iOrder in [19].

ent wireless interference models in literature [9]. In addition to interference model, LQF takes as input the link demand vector $f = (f_1, f_2, \dots, f_L)$ for L number of links, where the demand f_i for the i -th link is the number of packets to be transmitted across the link. The output of LQF is a schedule $S = \{S_1, S_2, \dots, S_\tau\}$, where S_j is a set of links scheduled in the j -th time slot. LQF works as follows to generate the output schedule:

1. Order and rename links such that $f_1 \geq f_2 \geq \dots \geq f_L$.
2. Set $i = 1, S = \emptyset, \tau = 0$. (Note: initial schedule is empty.)
3. Schedule link i in the very first available time slot to which link i can be added based on certain scheduling objective (e.g., guaranteeing certain minimum link reliability or maximizing network throughput) and interference model. If no such slot exists, increment τ and schedule link i in the newly created slot. (Note: incrementing τ is equivalent to creating a new empty slot at the end of the current schedule.)
4. Repeat step 3 f_i times.
5. Increment i . Go back to step 3 until $i > L$.

For scheduling based on the SINR model, we can use LQF without any modification [9], [36], and we only need to instantiate LQF in the following manner: at step 3, link i can be added to a slot j if 1) the SINR at all the receivers and senders of the slot is above certain threshold γ_0 when the scheduling objective is to guarantee certain minimum link reliability, or 2) if adding link i can increase the expected throughput in slot j when the scheduling objective is to maximize network throughput only. For convenience, we denote this SINR-based scheduling algorithm LQF_{sinr} .

For PRK-based scheduling, we need to extend LQF to accommodate the special properties of the PRK model. Given two links l and l' , we define the s-distance from l to l' , denoted by $sd(l, l')$, as $\min_{n \in \{l.t, l.r\}, n' \in \{l'.t, l'.r\}} sd(n, n')$ where $l.t$ and $l'.t$ are the transmitter of l and l' respectively and $l.r$ and $l'.r$ are the receiver of l and l' respectively. Accordingly, for any three links $l, l',$ and l'', l'' is regarded s-closer to l' than l is if $sd(l'', l') < sd(l, l')$. Then, for every link i' in a slot S_j in PRK-based scheduling, the s-radius of the exclusion region of i' in S_j is less than $\min_{l \in S_j, l \neq i'} sd(l, i')$. When link i cannot be added to any of the existing slots in step 3 of LQF, link i (more precisely, the transmitter and/or the receiver of i) may be within the exclusion region of another link already scheduled. When the scheduling objective is to ensure certain minimum link reliability, link i is within the exclusion region of another link i' in a slot S_j if 1) there is no other link $i'' \in S_j$ that is s-closer to i' than i is, and 2) the SINR at the transmitter or receiver of i' becomes less than certain threshold γ_0 (to violate the link reliability requirement) if we add i to S_j . When the scheduling objective is to maximize network throughput, link i is regarded as within the exclusion region of link i' in S_j if 1) there is no other link $i'' \in S_j$ that is s-closer to i' than i is, and 2) the local throughput of i' decreases if we add i to S_j , where the local throughput of i' is defined as $T_{i'}$ (see Formula 5) divided by the number of nodes in the exclusion region of i' . If i is within the exclusion region of i' , we say that the exclusion region of i' covers i .

Let S' be the set of existing slots when link i is being scheduled in step 3 of LQF but cannot be added into any one of S' . Had S' only include one slot S_j ($j = 1, 2, \dots, |S'|$), then according to the definition of the PRK model, for every link $i' \in S_j$ whose exclusion region covers i , we should remove from S_j every link $i'' \in S_j$, if any, with $sd(i'', i') = sd(i, i')$ so that the exclusion region of i' is well defined in S_j according to the PRK model; this is because, in the PRK model, all the concurrent transmitters of certain s-distance to a transmitter or receiver R , denoted by S_0 , are regarded as interferers to R and need to be silenced as long as any node in S_0 has to be silenced for ensuring certain ACK or packet reception reliability at R ; we denote all such removed links as $\mathbb{L}(S_j, i)$, and note that $\mathbb{L}(S_j, i)$ may be empty. To make the exclusion region of every link in every slot of S' well defined while minimizing the number of links that have to be removed from the existing slots (for the purpose of high throughput), we need to find the slot $S_{j'}$ such that $|\mathbb{L}(S_{j'}, i)| \leq |\mathbb{L}(S_j, i)|$ for all $j = 1, 2, \dots, |S'|$; then we regard link i as being silenced by some link $i' \in S_{j'}$, which entails the generation of a new slot for i . We denote $\mathbb{L}(S_{j'}, i)$ as $\mathbb{L}(i)$; to conform to the PRK model, we need to reschedule every link in $\mathbb{L}(i)$, if non-empty, in step 3 of LQF. Therefore, the PRK-based instantiation of LQF becomes as follows, which is the same as LQF_{sinr} except for the italicized part of step 3:

1. Order and rename links such that $f_1 \geq f_2 \geq \dots \geq f_L$.
2. Set $i = 1, S = \emptyset, \tau = 0$.
3. Schedule link i in the very first available time slot to which link i can be added based on certain scheduling objective and PRK interference model. If no such slot exists, increment τ and schedule link i in the newly created slot; *additionally, remove $\mathbb{L}(i)$, if non-empty, from an existing slot and reschedule them using step 3.*
4. Repeat step 3 f_i times.
5. Increment i . Go back to step 3 until $i > L$.

For convenience, we denote this algorithm as LQF_{prk} .

C. Experimental results

In what follows, we present the measurement results for NetEye and MoteLab respectively.

NetEye testbed. Using the scheduling algorithms LQF_{prk} and LQF_{sinr} , we have measured the performance of PRK- and SINR-based scheduling using the methodology discussed in Section V-A. Figures 15 and 16 show the PDR and end-to-end throughput of PRK- and SINR-based scheduling in the grid network and the random network respectively, with the error bars representing the 95% confidence intervals (which are very small) of the corresponding metrics. The PDR is defined as the number of successfully delivered packets divided by the number of packets transmitted in a schedule; the end-to-end throughput is defined as the number of successfully delivered packets divided by the schedule length (i.e., number of slots used in a schedule).¹¹ Note that the throughput is not that high because of the limited concurrency allowed in the testbed

¹¹We have also comparatively studied the PDRs of individual links as well as the spatial throughput in PRK- and SINR-based scheduling, and we observe similar phenomena as shown in Figures 15(a) and 16(a). Thus we only present data on end-to-end behavior here.

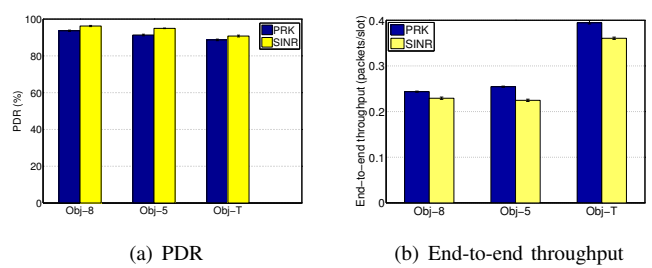
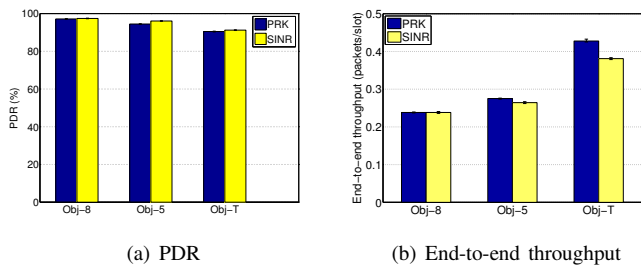


Fig. 15: PDR and end-to-end throughput in NetEye grid network

Fig. 16: PDR and end-to-end throughput in NetEye random network

# of Concurrent Links	1	2	3
Probability	0.46	0.51	0.03

TABLE II: Probability of having different number of concurrent links in a slot: random network, PRK, *Obj-8*

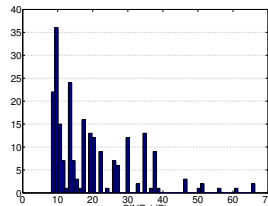


Fig. 17: Histogram of receiver-side SINRs in a PRK schedule for the random network and *Obj-8*

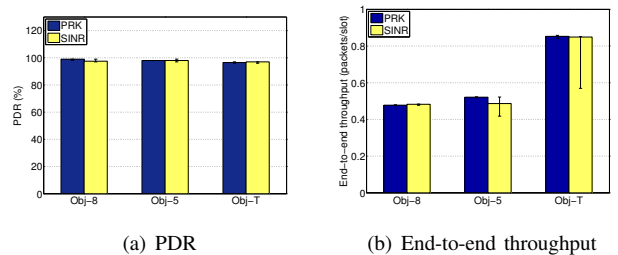


Fig. 18: PDR and end-to-end throughput in MoteLab

which is in turn due to the wide transitional region of wireless communication as can be seen from Figure 11. For instance, Table II shows the probability of having different number of concurrent links in a slot in PRK-based scheduling for the random network and the *Obj-8* objective.

We see that, in agreement with our analytical results, there is inherent tradeoff between reliability and throughput in both PRK- and SINR-based scheduling. As the scheduling objective moves from *Obj-8* to *Obj-5* and to *Obj-T*, for instance, the throughput in PRK- and SINR-based scheduling keeps increasing, but the PDR keeps decreasing accordingly. We also see that the performance of PRK-based scheduling is very close to that of SINR-based scheduling, thus the PRK model is able to address the drawbacks of the ratio-K model as observed in [9]. The PDRs of PRK- and SINR-based scheduling are above the required link reliability for objectives *Obj-8* and *Obj-5* except for cases that we will discuss in the next paragraph. The PDR in PRK-based scheduling is slightly lower than that in SINR-based scheduling, but the throughput tends to be higher in PRK-based scheduling. The reason why PRK-based scheduling tends to have slightly lower PDR and higher throughput is because PRK schedules are slightly shorter (e.g., by 3-4 slots less) than SINR schedules, and this is enabled by the fact that silencing/removing links closer-by in the PRK model allows more concurrently transmitting remote links (as discussed in Proposition 5).

Note that the measured PDRs of the PRK and SINR schedules slightly differ, sometimes higher and sometimes lower, from the PDRs predicted via the radio model and the required SINR threshold when we run the scheduling algorithms LQF_{prk} and LQF_{sinr} . This is because 1) wireless link properties (e.g., attenuation) change over time, and the schedule generated based on historical trace data may well behave differently as network condition changes, 2) the radio model itself evolves

over time [37], and 3) the generated schedule may not be the tightest tessellation of concurrent transmitters, and the SINR at receivers of a schedule may well be greater than the required minimum SINR threshold as shown in Figure 17. Therefore, it is important to adapt to in-situ network and environment conditions in scheduling. It is expected that the locality and high fidelity of the PRK model will enable new approaches to distributed, interference-oriented MAC protocol design, and we will study this issue in our future work.

Together with the above factors, the fact that LQF_{sinr} and LQF_{prk} are approximate algorithms and do not guarantee the optimality of the resulting schedules also explains why PRK schedules have slightly lower PDRs and higher throughput than SINR schedules even though the latter should have higher PDRs based on the analysis of Section IV. For instance, both PRK and SINR schedules ensure the minimum SINR threshold at receivers, but the actual SINRs at the receivers of SINR schedules are higher than those in PRK schedules; thus PDRs are higher in SINR schedules, and the reliability-throughput tradeoff leads to lower throughput in SINR-based scheduling.

MoteLab testbed. Even though the network, traffic, and environmental settings are different for NetEye- and MoteLab-based measurement studies, we observe similar phenomena in MoteLab as those in NetEye. For instance, Figure 18 shows the PDR and throughput for PRK- and SINR-based scheduling in MoteLab. The figure shows the tradeoff between link reliability and network throughput in scheduling; it also shows that PRK-based scheduling enables a throughput similar to what is feasible in SINR-based scheduling while ensuring the required link reliability.

VI. RELATED WORK

Maheshwari et al. [9] and Moscibroda et al. [17] have studied the benefits of SINR-based scheduling as compared with ratio-

K-based scheduling. Without studying the impact of different factors and the tradeoff between reliability and throughput in ratio-K-based scheduling, however, these work did not study how to best use the ratio-K model. Focusing on wireless sensing and control networks and based on comprehensive study of the behavior of ratio-K-based scheduling (in particular, the tradeoff between reliability and throughput), we propose the PRK interference model as a basis of adapting K to network and environmental dynamics in ratio-K-based scheduling. We have also studied the optimality of PRK-based scheduling through analysis, simulation, and testbed-based measurement.

Most closely related to our work is Shi et al. [18] who, in parallel with our study, examined the effectiveness of the protocol interference model for frequency scheduling (together with routing and power control). Having not focused on distributed protocol design, however, Shi et al. left it as a challenging open problem on how to efficiently choose optimal K in instantiating the ratio-K model, and the optimal K was searched by solving a series of centralized optimization problems in [18]. Through detailed study on the sensitivity of and the inherent tradeoff between throughput and reliability in ratio-K-based scheduling, we discover the simple, distributed, link reliability-based approach to instantiating the ratio-K model, and we propose the PRK model which has both the locality of the ratio-K model and the high fidelity of the SINR model. Orthogonal to the focus of Shi et al. [18], our work also examines the effectiveness of ratio-K-based scheduling from the perspective of time scheduling and distributed protocol design, studies why PRK/ratio-K-based scheduling can be very close to the performance of SINR-based scheduling, examines the issue in wireless sensing and control networks with a wide range of system configurations (on factors such as traffic load, link length, and wireless signal attenuation), and corroborates the analytical and simulation results with testbed-based measurement.

Other approximate interference models such as hop-based model [38] and range-based model [34] have also been used in the literature, but they are either similar or inferior to the ratio-K model [9]. Therefore, we did not study those approximate models in this paper. Katz et al. [39] studied the feasibility of local interference model, where only nodes in a local neighborhood (with diameter ρ) need to coordinate with one another to ensure minimum SINR at each receiver. But they did not study the impact of various factors on the optimal ρ , nor did they study how to correctly instantiate ρ in dynamic, potentially unpredictable network and environmental settings. Spatial reuse control based on the concept of exclusion region has been studied too [40], [41]. Nonetheless, the issue of the optimal Ks in different scenarios and the comparison between ratio-K- and SINR-based scheduling were not studied in these work. Most of these work have also only focused on exclusion regions around receivers, but not on exclusion regions around both the transmitters and receivers of data transmissions at the same time to ensure reliable delivery of both data and ACK.

VII. CONCLUDING REMARKS

Through detailed analysis of how different network and environmental factors, such as traffic load and wireless sig-

nal attenuation, affect the optimal instantiation of the ratio-K model, we showed that the performance of ratio-K-based scheduling is highly sensitive to the choice of K and that it is important to take this into account in both protocol design and performance evaluation. We then comparatively studied the performance of PRK- and SINR-based scheduling and showed that, if correctly instantiated via the PRK model, ratio-K-based scheduling can achieve a close-to-optimal performance. Our findings on PRK-based scheduling and the inherent tradeoff between reliability and throughput suggest that the ratio-K model can be optimally instantiated through link-reliability-based adaptation of K, which is amenable to distributed, local implementation too. These findings showed the feasibility of integrating the high fidelity of the SINR model with the locality of the ratio-K model, and suggested new approaches to MAC protocol design in dynamic, unpredictable network and environmental settings. Thus these findings opened up new opportunities and perspectives on interference-oriented protocol design and analysis in wireless sensing and control networks, and we will explore these opportunities in our future work.

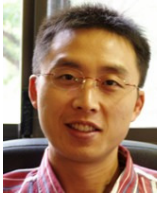
REFERENCES

- [1] K. Chintalapudi and L. Venkatraman, "On the design of mac protocols for low-latency hard real time latency applications over 802.15.4 hardware," in *ACM/IEEE IPSN*, 2008.
- [2] WirelessHART, http://www.hartcomm2.org/hart_protocol/wireless_hart/wireless_hart_main.html.
- [3] ISA SP100.11a, <http://www.isa.org/MSTemplate.cfm?MicrositeID=1134&CommitteeID=6891>.
- [4] F. Tobagi and L. Kleinrock, "Packet switching in radio channels: Part ii—the hidden terminal problem in carrier sense multiple-access and the busy-tone solution," *IEEE Transactions on Communications*, vol. COM-23, no. 12, pp. 1417–1433, 1975.
- [5] G. Zhou, T. He, J. A. Stankovic, and T. Abdelzaher, "RID: Radio interference detection in wireless sensor networks?" in *IEEE INFOCOM*, 2005.
- [6] H. Zhang, A. Arora, and P. Sinha, "Link estimation and routing in sensor network backbones: Beacon-based or data-driven?" *IEEE Transactions on Mobile Computing*, vol. 8, no. 5, May 2009.
- [7] P. Gupta and P. R. Kumar, "The capacity of wireless networks," *IEEE Transactions on Information Theory*, vol. 46, no. 2, 2000.
- [8] G. Sharma, R. R. Mazumdar, and N. B. Shroff, "On the complexity of scheduling in wireless networks," in *ACM MobiCom*, 2006.
- [9] R. Maheshwari, S. Jain, and S. Das, "A measurement study of interference modeling and scheduling in low-power wireless networks," in *ACM SenSys*, 2008.
- [10] G. Brar, D. M. Blough, and P. Santi, "The SCREAM approach for efficient distributed scheduling with physical interference in wireless mesh networks," in *ICDCS*, 2008.
- [11] Y. Yi, G. D. Veciana, and S. Shakkottai, "On optimal MAC scheduling with physical interference model," in *IEEE INFOCOM*, 2007.
- [12] L. Ying and S. Shakkottai, "Scheduling in mobile ad hoc networks with topology and channel-state uncertainty," in *IEEE INFOCOM*, 2009.
- [13] A. Arora, R. Ramnath, E. Ertin, P. Sinha, S. Bapat, V. Naik, V. Kulathurmani, H. Zhang, H. Cao, M. Sridhara, S. Kumar, N. Seddon, C. Anderson, T. Herman, N. Trivedi, C. Zhang, M. Gouda, Y. R. Choi, M. Nesterenko, R. Shah, S. Kulkarni, M. Aramugam, L. Wang, D. Culler, P. Dutta, C. Sharp, G. Tolle, M. Grimmer, B. Ferriera, and K. Parker, "Exscal: Elements of an extrem scale wireless sensor network," in *IEEE RTCSA*, 2005.
- [14] H. Zhang, A. Arora, Y. ri Choi, and M. Gouda, "Reliable bursty convergecast in wireless sensor networks," *Computer Communications (Elsevier), Special Issue on Sensor-Actuator Networks*, vol. 30, no. 13, 2007.
- [15] J. I. Choi, M. Jain, M. A. Kazandjieva, and P. Levis, "Granting silence to avoid wireless collisions," in *IEEE ICNP*, 2010.
- [16] D. Chafekar, V. A. Kumar, M. V. Marathe, S. Parthasarathy, and A. Srinivasan, "Approximation algorithms for computing capacity of wireless networks with sinr constraints," in *IEEE INFOCOM*, 2008.

- [17] T. Moscibroda, R. Wattenhofer, and Y. Weber, "Protocol design beyond graph based models," in *ACM HotNets*, 2006.
- [18] Y. Shi, Y. T. Hou, J. Liu, and S. Kompella, "How to correctly use the protocol interference model for multi-hop wireless networks," in *ACM MobiHoc*, 2009.
- [19] X. Che, X. Liu, X. Ju, and H. Zhang, "Adaptive instantiation of the protocol interference model in mission-critical wireless networks," Wayne State University (<https://sites.google.com/site/dnctr/DNC-TR-08-04.pdf>), Tech. Rep. WSU-CS-DNC-TR-08-04, December 2008.
- [20] T. Rappaport, *Wireless Communications*. Prentice-Hall, Upper Saddle River, NJ, 2002.
- [21] W. Niu, J. Li, and T. Talty, "Intra-vehicle UWB channel measurements and statistical analysis," in *IEEE GlobeCom*, 2008.
- [22] "IEEE Std 802.15.4-2006," Wireless Medium Access Control (MAC) and Physical Layer (PHY) Specifications for Low-Rate Wireless Personal Area Networks (WPANs), September 2006.
- [23] G. Zhou, T. He, S. Krishnamurthy, and J. Stankovic, "Models and solutions for radio irregularity in wireless sensor networks," *ACM Transactions on Sensor Networks*, vol. 2, no. 2, 2006.
- [24] T. Tabet and R. Knopp, "Spatial throughput of multi-hop wireless networks under different retransmission protocols," in *Allerton*, 2004.
- [25] D. Stoyan, W. S. Kendall, and J. Mecke, *Stochastic Geometry and its applications*. Wiley, 1995.
- [26] K. Sohrabi, B. Manriquez, and G. J. Pottie, "Near ground wideband channel measurement."
- [27] J. Hellerstein, Y. Diao, S. Parekh, and D. M. Tilbury, *Feedback Control of Computing Systems*. Wiley-IEEE Press, 2004.
- [28] "NetEye testbed," <http://neteye.cs.wayne.edu/neteye/home.php>.
- [29] G. Werner-Allen, P. Swieskowski, and M. Welsh, "Motelab: A wireless sensor network testbed," in *IEEE/ACM IPSN/SPOTS*, 2005.
- [30] C. Joo, X. Lin, and N. B. Shroff, "Understanding the capacity region of the greedy maximal scheduling algorithm in multi-hop wireless networks," in *IEEE INFOCOM*, 2008.
- [31] L. B. Le, E. Modiano, C. Joo, and N. B. Shroff, "Longest-queue-first scheduling under SINR interference model," in *ACM MobiHoc*, 2010.
- [32] D. M. Blough, S. Das, G. Resta, and P. Santi, "A framework for joint scheduling and diversity exploitation under physical interference in wireless mesh networks," in *IEEE MASS*, 2008.
- [33] G. Brar, D. M. Blough, and P. Santi, "Computationally efficient scheduling with the physical interference model for throughput improvement in wireless mesh networks," in *ACM MobiCom*, 2006.
- [34] W. Wang, Y. Wang, X.-Y. Li, W.-Z. Song, and O. Frieder, "Efficient interference-aware TDMA link scheduling for static wireless networks," in *AMC MobiCom*, 2006.
- [35] X. Che, X. Ju, and H. Zhang, "The case for addressing the limiting impact of interference on wireless scheduling," in *IEEE ICNP*, 2011.
- [36] R. Maheshwari, J. Cao, and S. Das, "Physical interference modeling for transmission scheduling on commodity wifi hardware," in *IEEE INFOCOM miniconference*, 2009.
- [37] M. Sha, G. Xing, G. Zhou, S. Liu, and X. Wang, "C-MAC: Model-driven concurrent medium access control for wireless sensor networks," in *IEEE INFOCOM*, 2009.
- [38] I. Rhee, A. Warrier, J. Min, and L. Xu, "DRAND: Distributed randomized TDMA scheduling for wireless ad hoc networks," in *ACM MobiHoc*, 2006.
- [39] B. Katz, M. Volker, and D. Wagner, "Link scheduling in local interference models," in *AlgoSensors*, 2008.
- [40] R. Menon, R. M. Buehrer, and J. H. Reed, "Impact of exclusion region and spreading in spectrum-sharing ad hoc networks," in *ACM Workshop on Technology and Policy for Accessing Spectrum*, 2006.
- [41] H. Ma, H. M. Alazemi, and S. Roy, "A stochastic model for optimizing physical carrier sensing and spatial reuse in wireless ad hoc networks," in *IEEE MASS*, 2005.

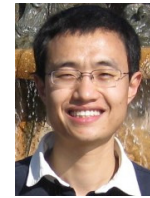


Xin Che (S'10) received his B.S. and M.S. in Electrical Engineering as well as his B.S. in Computer Science from Huazhong University of Science and Technology. He is currently pursuing his Ph.D. degree in Computer Science at Wayne State University. His primary research interests lie in modeling, algorithmic, and systems issues in wireless, embedded, and sensor networks.



Award. (URL: <http://www.cs.wayne.edu/~hzhang>).

Hongwei Zhang (S'01-M'07/ACM S'01-M'07) received his B.S. and M.S. degrees in Computer Engineering from Chongqing University, China and his Ph.D. degree from The Ohio State University. He is currently an assistant professor of computer science at Wayne State University. His primary research interests lie in the modeling, algorithmic, and systems issues in wireless, vehicular, embedded, and sensor networks. His research has been an integral part of several NSF, DARPA projects such as the KanseiGenie and ExScal projects. He is a recipient of the NSF CAREER



Xi Ju received his M.S. and Ph.D. degrees in Computer Science from Southeast University, China. He is currently a visiting scholar of computer science at Wayne State University. His research focuses on wireless, vehicular, and embedded networked sensing. He has been involved in the development of the Chinese Next Generation Internet and the US NSF GENI project.



Xiaohui Liu received his B.S. degree in Computer Science from Wuhan University, China. He is currently a PhD candidate of computer science at Wayne State University. His primary research interests lie in real-time, QoS routing in wireless and sensor networks. He is a student member of ACM.